Spin structure in perpendicularly magnetized Fe-FePt bilayers

B. Laenens,[1,*] N. Planckaert,[1] J. Demeter,[1] M. Trekels,[1] C. L'abbé,[2] C. Strohm,[3] R. Rüffer,[3] K. Temst,[1] A. Vantomme,[1] and J. Meersschaut[1,4]

[1]*Instituut voor Kern- en Stralingsfysica and INPAC, K.U.Leuven, Celestijnenlaan 200 D, B-3001 Leuven, Belgium*

[2]*Hogeschool voor Wetenschap en Kunst-Campus De Nayer, Jan de Nayerlaan 5, B-2860 Sint-Katelijne-Waver, Belgium*

[3]*European Synchrotron Radiation Facility, BP 220, F-38043 Grenoble Cedex, France*

[4]*imec, Kapeldreef 75, B-3001 Leuven, Belgium*

(Received 28 October 2008; revised manuscript received 19 July 2010; published 17 September 2010)

We studied the exchange-spring behavior in FePt-Fe hard-soft magnetic heterostructures. We present a study of the spin structure of the soft Fe layer of Fe-FePt bilayers by nuclear forward scattering of synchrotron radiation. The orientation of the Fe moments close to the top of the soft layer was determined quantitatively as a function of the soft-layer thickness. We show that for a few monolayers of Fe, the magnetically hard FePt layer pins the magnetization in the soft Fe layer to the out-of-plane direction. With increasing Fe-layer thickness, the influence of the FePt diminishes and the magnetization cants toward the in-plane Fe[001] direction. The significance of the exchange coupling constant as the relevant parameter for the exchange-spring behavior is demonstrated by one-dimensional micromagnetic simulations.

DOI: 10.1103/PhysRevB.82.104421 PACS number(s): 75.25.−j, 75.70.−i, 76.80.+y

I. INTRODUCTION

The exchange-spring magnet, which is based on interfacial exchange-coupled soft and hard ferromagnetic materials, combines the high magnetization of the soft phase with the high magnetic anisotropy of the hard phase.[1] With advanced preparation techniques researchers aim to achieve spring magnets with high values of the maximum energy product and of the remanent magnetization.[2,3] This kind of system is of interest for low-cost permanent magnets and novel functional magnetic nanostructures. Fe-FePt bilayers are prototypes of exchange-spring magnets.[4–6] FePt in the $L1_0$ phase is a hard material with a high magnetocrystalline anisotropy[7,8] while Fe is a soft ferromagnetic material with a low anisotropy and high spontaneous magnetization. So far, experimental studies mainly concentrated on thin exchange-spring bilayers with both the hard and the soft magnetic moments oriented in the film plane.[4,9–12]

Nowadays, the focus is on magnetic structures having the easy magnetization axis orthogonal to the film plane. Epitaxial FePt thin films stabilized in the $L1_0$-crystal structure show this property when grown on MgO(100).[13–17] Moreover, by depositing a thin Fe film onto a $L1_0$ FePt layer, an interesting phenomenon appears: while the hard FePt layer forces its magnetization perpendicular to the film plane, the soft Fe layer tends to orient its magnetic moments in the plane. This perpendicular exchange coupling is an interesting field of study with direct applications in the ultrahigh density magnetic recording industry.[18–20] Casoli *et al.*[5,21] macroscopically studied the exchange interaction between the hard FePt and the soft Fe phases via measuring the orthogonal magnetization of Fe-FePt bilayers as a function of the external field. On the microscopic scale, little is known about the spin structure within this system.

The spin structure inside the soft and the hard layers can be theoretically modeled by means of micromagnetic calculations both for lateral exchange-spring systems[1,9,22] as well as for perpendicular magnets.[6,23] In perpendicular exchange-spring bilayers the moments of the soft phase are predicted to vary from along the sample normal to along the in-plane direction as the distance of the moments from the interface is increased. However, experimental evidence for this gradual spin rotation is lacking. In this work, we experimentally study the magnetic moment orientation in the soft phase of Fe-FePt.

A local probing of the magnetization inside the Fe layer of Fe-FePt bilayers is possible via nuclear-resonant scattering of synchrotron radiation (NRS). NRS, being a time analog to classical Mössbauer spectroscopy, is sensitive to Mössbauer nuclei only. The high brilliance of third generation synchrotron sources allows one to probe very thin and even monoatomic probe layers of the resonant isotope ^{57}Fe within a nonresonant sample. The use of an inclined probe layer and the ability to focus the beam down to micrometer size makes it possible to address different depths within the same sample by lateral displacement of the beam. The combination of the high brilliance, the isotope sensitivity and the use of very small beams make NRS a unique tool for the study of magnetic nanostructures.[4,24–26]

II. EXPERIMENTAL

An Fe-FePt bilayer is prepared by molecular-beam epitaxy onto a preannealed MgO(100) substrate. The substrate is $20\times20\times2$ mm^3 in size. The pressure during growth remained below 5×10^{-10} Torr. We used calibrated quartz crystal monitors to control the thickness, the deposition rate, and the relative atomic flux. The deposition rates for ^{56}Fe and Pt were 0.029 Å/s and 0.039 Å/s, respectively. The ^{56}FePt film with a nominal thickness of 30 nm was prepared at a temperature of 500 °C and contains the nonresonant isotope ^{56}Fe. The elevated temperature results in a highly ordered and magnetically hard $L1_0$ phase with perpendicular magnetization.[15] As illustrated in Fig. 1, a tilted probe layer of ^{57}Fe (0.7 nm) was prepared onto an ^{56}Fe-wedge-shaped layer. The wedge was prepared by linearly moving a shutter

 ©2010 The American Physical Society

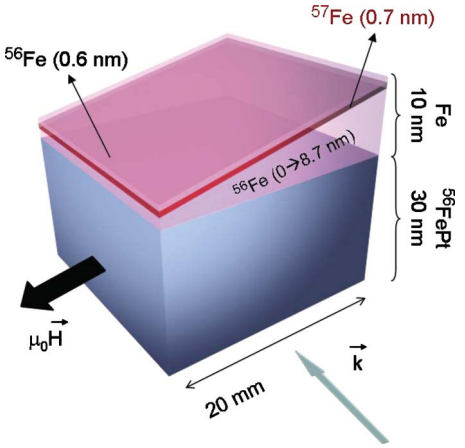

FIG. 1. (Color online) Representation of the investigated Fe-FePt bilayer. An ^{57}Fe probe layer is grown on the wedged shape. The direction of the external applied field $\mu_0\vec{H}$ and the direction of the synchrotron beam $\vec{k}$ with respect to the sample are indicated.

plate in front of the sample. The wedged probe layer allows one to study the moments in the top monolayers of the Fe layer as a function of the soft-layer thickness by growing one single-bilayer system with unique properties of the hard layer. The Fe structure was deposited at 100 °C. The sample was capped with an additional layer of ^{56}Fe (0.6 nm) and a protecting layer of Ag (3 nm).

The crystallographic structure and the texture of the thin film was characterized by high angle x-ray diffraction (XRD) experiments. An x-ray diffractometer with a Cu x-ray source [$K\alpha$(Cu)=1.5401 Å] was used. Figure 2(a) displays the XRD scan of the Fe-FePt bilayer. The $K\beta$ and $K\alpha$ x-ray reflections on the substrate result in the diffraction peaks at 38.65° and 42.97°, respectively. The diffraction peaks at 2θ =24.0°, 49.1°, and 77.2° are attributed to the (001), (002), and (003) reflections of the $L1_0$ crystal. The presence of only (00n) diffraction peaks indicates that the FePt is textured in the FePt[001] direction perpendicular to the substrate and that the film grows epitaxially on MgO(100). The results are in agreement with earlier work on $L1_0$-FePt thin films directly grown on MgO(100) substrates.[15] The diffraction peak around 64.0° shows that the Fe layer is in the bcc-crystal phase.

The in-plane structure and epitaxial relations were explored by asymmetric diffraction scans. Figure 2(b) shows two ϕ scans of the Fe-FePt bilayer. The spectra indicate the measured Fe(110) (2θ=44.76°) and FePt(101) (2θ=33.06°) intensities at 45° from the sample normal while rotating the bilayer thin film about the sample normal. The offset between adjacent Fe(110) and FePt(101) peaks being 45° confirms that the bcc-Fe unit cell grows at 45° rotated in plane with respect to the $L1_0$-FePt unit cell. Further, we found that the Fe unit cell is rotated 45° with respect to the MgO substrate (for the epitaxial relations between MgO and FePt we refer to the pole figures in Ref. 15). The epitaxial relations between the Fe, the FePt, and the MgO unit cells are illustrated in the inset of Fig. 2(b). The slope of the Fe wedge is aligned with one of the edges of the MgO substrate. As illustrated in Fig. 1, the synchrotron beam $\vec{k}$ is aligned perpendicularly to this wedge. Thus, the beam points along the crystallographic [110] direction of the bcc-Fe layer or, in other words, the angle between $\vec{k}$ and Fe[100] is 45°.

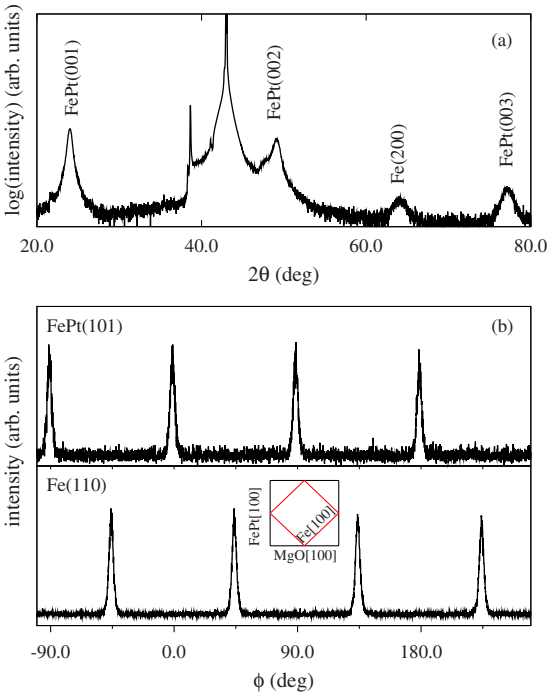

FIG. 2. (Color online) (a) X-ray diffraction (θ-2θ) scan of the Fe-FePt bilayer on MgO(100). (b) Fe(110) and FePt(101) intensities at 45° from the sample plane normal as a function of rotation angle ϕ about the surface normal. The inset illustrates the epitaxial relation between bcc-Fe, $L1_0$-FePt, and the substrate.

We investigated the macroscopic magnetic properties of the Fe-FePt bilayer at room temperature by means of vibrating sample magnetometry. The sample for the measurement of the bulk magnetization was cut into three parts perpendicular to the slope of the wedge. The magnetization curves look similar as the loops reported by Casoli *et al.*,[5] i.e., as the soft-layer thickness increases, the perpendicular remanence decreases. The moments of the bilayer could not be saturated in the film plane with the maximum available field of 9 T.

The magnetic-moment orientation in the ^{57}Fe layers of the Fe-FePt bilayer was investigated at room temperature by means of nuclear-resonant scattering of synchrotron radiation. The sample was placed in grazing-incidence geometry and measurements were performed at beamline ID18 of the ESRF (Ref. 27) both in zero field and with an external field applied parallel to the thin-film plane but perpendicular to the synchrotron beam (see Fig. 1). The width of the beam at the sample position was 60 μm so that the depth resolution is mainly determined by the thickness of the probe layer (being 0.7 nm). The energy of the beam was monochromatized to 14.413 keV. This is the energy of the magnetic dipole transition of ^{57}Fe with spins $I_g=1/2$ and $I_e=3/2$. Synchrotron radiation, incident on the sample, will simultaneously excite the hyperfine-split nuclear energy levels of the ^{57}Fe atoms. The intensity of the delayed photons is recorded as a function of time. Apart from a decaying intensity related to the lifetime of the excited state (141 ns in the case of ^{57}Fe),

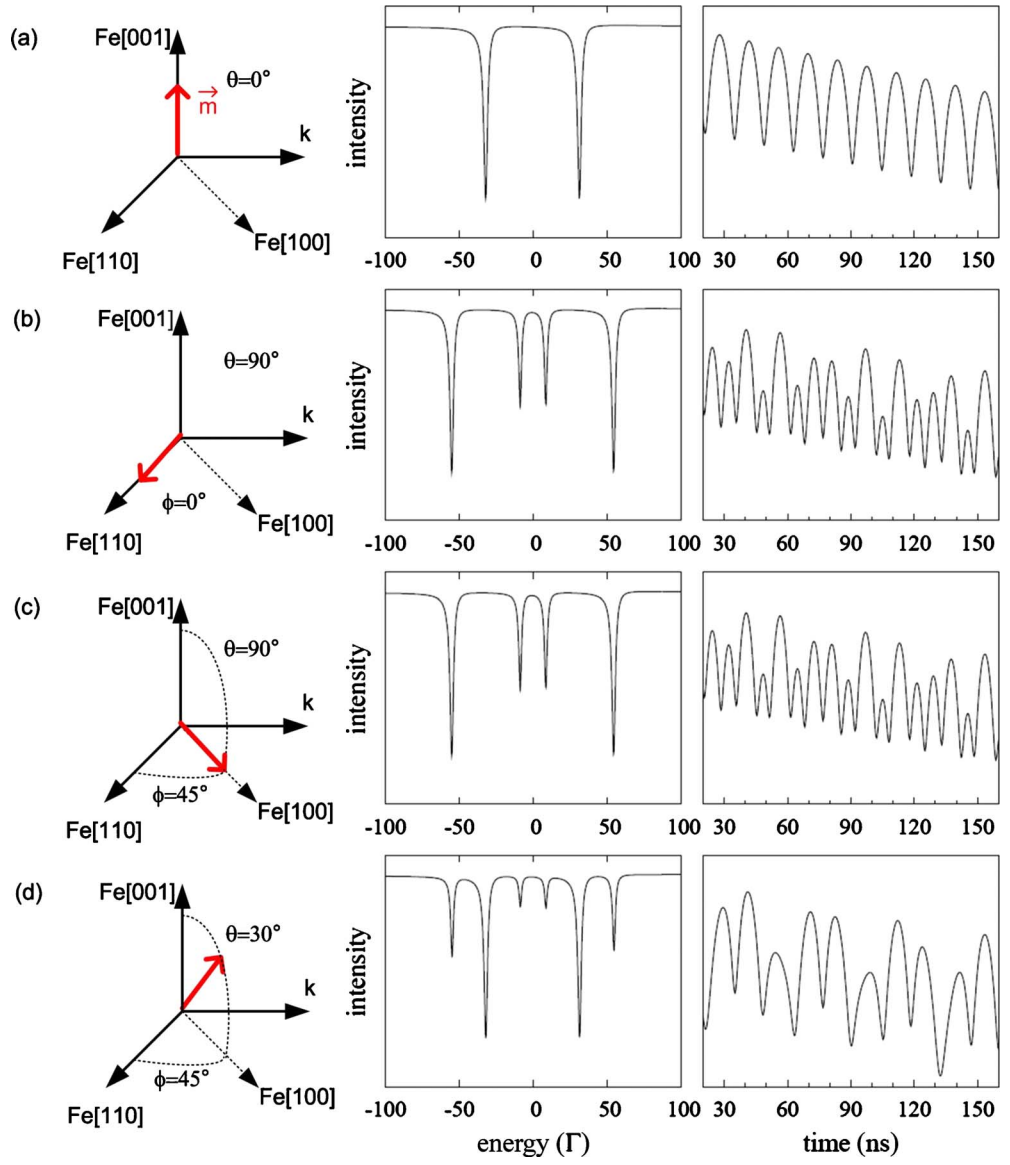

FIG. 3. (Color online) Right column: simulated time spectra for different orientations of the magnetic moments relative to the beam direction and the bcc-Fe axes. $\vec{k}$ is a vector along the photon beam and Fe[001] is aligned with the sample normal. The ($\vec{k}$,Fe[110]) plane lies in the plane of the synchrotron. The polar angle θ is defined as the angle between the sample normal, Fe[001], and the magnetic moment $\vec{m}$. The azimuthal angle ϕ is the angle between Fe[110] and the projection of $\vec{m}$ in the sample plane. The simulations are obtained by the program CONUSS (Ref. 29) for an ^{57}Fe(2.0 nm) thin film. The model consists of four hyperfine sites with the same hyperfine field strength of −33 T. Yet, they have different but complementary orientations: $m_1(\theta,\phi)$, $m_2(\pi-\theta,\phi)$, $m_3(\theta,2\pi-\phi)$, and $m_4(\pi-\theta,2\pi-\phi)$. The spectra in the second column show the nuclear-resonance lines in energy-domain relative to 14.413 keV (Γ=4.65 neV).

the time spectra show rapid oscillations, i.e., quantum beats, originating from the hyperfine splitting of the nuclear states. The strength of the splitting is proportional to the total magnetic field at the position of the nucleus, which is the sum of the hyperfine field and the externally applied field. In the case of ^{57}Fe, the magnetic hyperfine field vector is antiparallel to the net atomic magnetic moment $\vec{m}$. Hence, knowledge of the direction of the magnetic hyperfine field implies the knowledge of the direction of the spin orientation.[28]

The quantum beat pattern depends strongly on the relative orientation of the magnetic moments $\vec{m}$ with respect to the direction and polarization of the incident synchrotron radiation (here, the magnetic field of the incident synchrotron radiation is along the sample normal). This is illustrated by the simulated time spectra in Fig. 3. The simulations are obtained by the program CONUSS (Ref. 29) for an ^{57}Fe(2.0 nm) thin film. When $\vec{m}$ is along the sample normal [Fig. 3(a), θ =0°], only the nuclear transitions which require an angular-momentum change Δm=0 can be excited, i.e., the two transitions depicted in the energy spectrum of Fig. 3(a). In the time domain, the interference between the two nuclear transitions results in a beating pattern with a single frequency. When the angle θ between the sample normal and $\vec{m}$ increases, additional nuclear transitions are allowed, each with a different weight. Consequently, the time spectrum shows multiple frequencies [see Figs. 3(b)–3(d)].

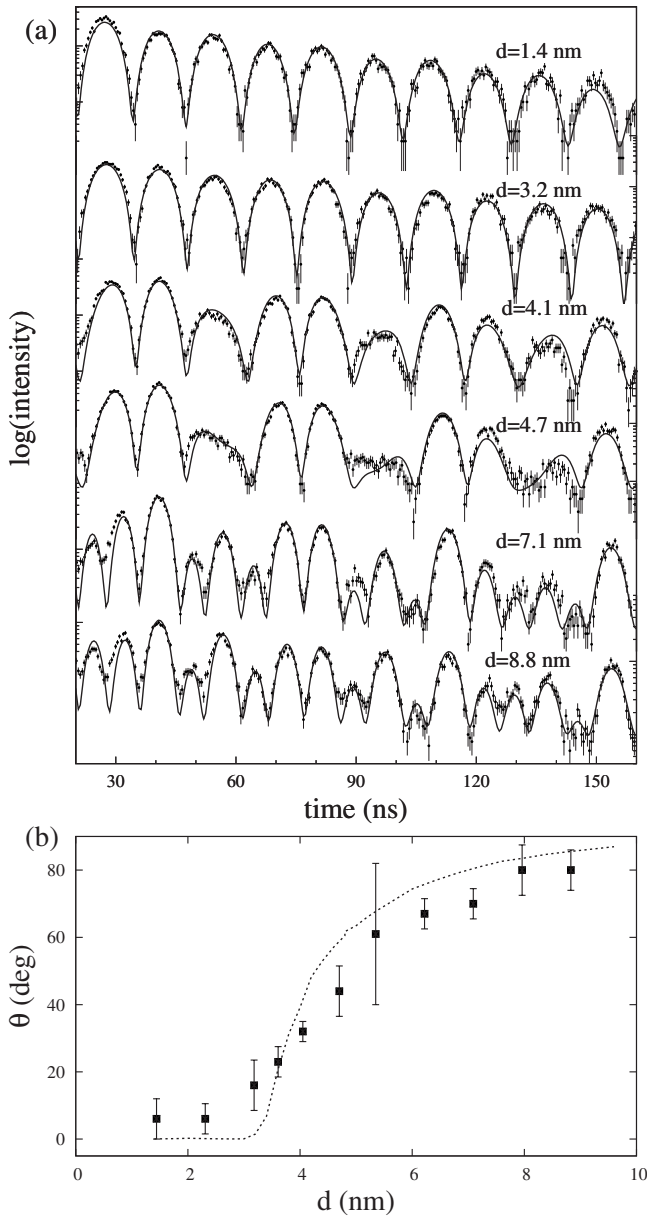

FIG. 4. (a) Selection of time spectra of the wedged Fe-FePt bilayer. The parameter d is varied by changing the lateral position of the focused synchrotron beam onto the canted ^{57}Fe(0.7 nm) probe layer. The spectra are recorded at zero field and at room temperature. The solid lines are the fits obtained by the fitting program CONUSS (Ref. 29). (b) Dependence of the spin rotation in the Fe layers on the distance d from the FePt interface. The angles θ are extracted from the fits of the NRS time spectra. The dashed line represents the simulation result as discussed in the text.

III. MICROSCOPIC SPIN STRUCTURE

To investigate the local Fe magnetization in the top monolayers of the Fe layer as a function of the soft-layer thickness, the focused synchrotron beam was aligned at 11 positions on the ultrathin ^{57}Fe (0.7 nm) probe layer. At these positions time spectra were recorded under grazing incidence conditions. Figure 4(a) shows a selection of the recorded time spectra. We denote the distance of the probe atoms to the FePt interface with the parameter d. For the ^{57}Fe located at a distance of $d=1.4$ nm from the FePt interface, the time spectrum shows a pronounced beating pattern with a single frequency similar to the simulation for $\vec{m}$ along the sample normal in Fig. 3(a). The time evolution of the intensity changes to a pattern with multiple frequencies as the distance to the interface is increased.

To account for magnetic domain formation we defined complementary hyperfine-field sites in our model. These sites are characterized by the same hyperfine field strength, yet with different rotation angles, namely, $m_1(\theta,\phi)$, $m_2(\pi-\theta,\phi)$, $m_3(\theta,2\pi-\phi)$, and $m_4(\pi-\theta,2\pi-\phi)$, and they interfere coherently. Hence, the polar angle θ is defined as the angle between the sample normal and the magnetic moment. The azimuthal angle ϕ is the angle between Fe[110] and the projection of the vector $\vec{m}$ in the sample plane [see Figs. 3(c) and 3(d)]. The rotation of the vectors $\vec{m}_i$ is limited between two perpendicular easy axes of the bcc-Fe layer, for instance, Fe[001] and Fe[100], and thus $0<\theta<\pi/2$ and $\phi=45°$. Analysis of the quantum beats with this model permits an accurate determination of the local moment direction.

The analysis of the 11 time spectra with the NRS fitting interface[24] for CONUSS (Ref. 29) indicates a magnetic hyperfine field of −33 T with a Gaussian width of 1.7 T. From each spectrum a unique rotation angle θ is obtained. Figure 4(b) shows the rotation angles as a function of the distance to the FePt interface. At a distance to the FePt interface of less than 3 nm, the Fe moments are oriented perpendicular to the thin-film surface whereas at a distance of 9 nm they are almost parallel with the surface. In between, the moments gradually rotate from the out-of-plane to in-plane direction. Hence, we observe a clear exchange-spring behavior in the perpendicular direction.

The exchange-spring behavior could be simulated by the application of the Landau-Lifschitz equation of motion for the one-dimensional classical spin chain[30,31]

$$\frac{\partial \vec{M}_i}{\partial t} = \vec{M}_i \times \vec{F}_i - \gamma[\vec{M}_i \times (\vec{M}_i \times \vec{F}_i)]. \quad (1)$$

with γ a very small dimensionless dissipation constant and $\vec{M}_i$ the unit magnetization of the ith sublayer. We divided the Fe layer into N sublayers of thickness $t_{\mathrm{Fe}}=0.2$ nm such that $d=0.2\times N$. The FePt layer is kept as a single layer. $\vec{F}_i$ is the effective field related to the energy density W via $\vec{F}_i=-\partial W/\partial \vec{M}_i$. The energy density is the sum of several contributions. The Zeeman term is described by $W_{\mathrm{Zee}}=-\Sigma_{i=1}^{N}(\vec{M}_i\cdot\vec{H})t_{\mathrm{Fe}}m_{\mathrm{Fe}}+(\vec{M}_0\cdot\vec{H})t_{\mathrm{FePt}}m_{\mathrm{FePt}}$ with $\vec{M}_0$ the unit magnetization of the FePt layer. We used the magnetization per volume $m_{\mathrm{Fe}}=1.76\times10^6$ J/(T m^3) and $m_{\mathrm{FePt}}=1.14\times10^6$ J/(T m^3) for Fe and FePt, respectively.[1] For FePt the uniaxial anisotropy contribution to the total-energy density can be described by $W_{\mathrm{ani}}=\frac{1}{2}K_u t_{\mathrm{FePt}}\vec{M}_{0z}^2$ with $K_u=4\times10^6$ J/m^3. The cubic magnetocrystalline anisotropy of the Fe layer is described by $W_{\mathrm{ani}}=\Sigma_{i=1}^{N}K_c t(\vec{M}_{ix}^2\vec{M}_{iy}^2+\vec{M}_{iy}^2\vec{M}_{iz}^2+\vec{M}_{iz}^2\vec{M}_{ix}^2)$. Finally, we used the phenomenological model for exchange coupling: $W_{\mathrm{exc}}=-\Sigma_{i=0}^{N-1}J_a(\vec{M}_i\cdot\vec{M}_{i+1})^2$ with J_a the exchange coupling constant. Note that in this model J_a is

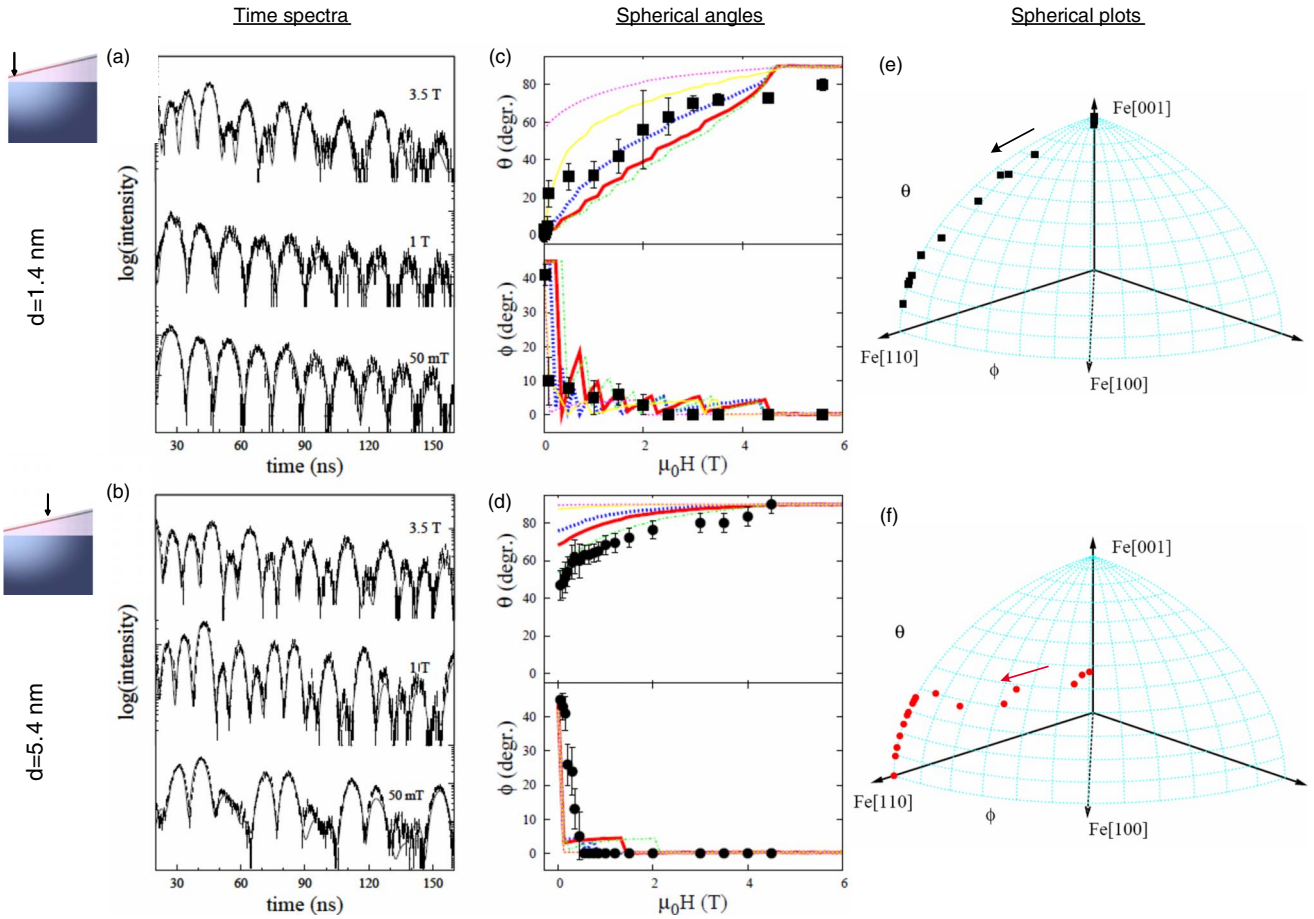

FIG. 5. (Color online) First column: time spectra taken in various external fields for the ^{57}Fe probe nuclei located at (top) $d=1.4$ nm and (bottom) $d=5.4$ nm from the FePt interface. The solid lines are the fits obtained by the fitting program CONUSS (Ref. 29). Second column: rotation angles ϕ and θ as a function of the external field for the moments located at a distance (■) $d=1.4$ nm and (●) $d=5.4$ nm of the FePt interface. The colored line represents the simulation result with $J=0.2\times10^{-11}$ J/m (magenta thin dotted line), 0.4×10^{-11} J/m (yellow thin solid line), 1.0×10^{-11} J/m (blue thick dotted line), 2.0×10^{-11} J/m (red thick solid line), and 3.0×10^{-11} J/m (green thin dot-dashed line). The oscillations seen in the simulation results for the angle ϕ are due to numerical noise ($W_{ani}\ll W$). The polar angles ϕ, θ and the direction of the applied field are defined in the text and illustrated in Fig. 3. Third column: the rotation of the moments shown in a spherical axis system. The arrows indicate the direction of the canting as the field increases. For the sake of clarity the error bars are omitted.

defined as the exchange coupling constant per sublayer thickness $t_{Fe}=0.2$ nm. Further we will report on the more commonly used exchange-spring constant per unit length J.

To reproduce the Fe wedge in the simulations, we increased the number of Fe sublayers $N:7\rightarrow28$ which corresponds with a thickness range of $14\rightarrow96$ nm. For each N, the Landau-Lifschitz equation was solved in the presence of external fields from −6 till 6 T. Finally the remanent magnetization was extracted. The dashed line in Fig. 4(b) is the result of simulations with exchange constant $J=2.0\times10^{-11}$ J/m. This value is obtained after analysis of the depth dependence of the magnetic spins in the probe layer and the magnetization curves discussed in the next paragraph. Moreover, the value is consistent with the results reported in literature.[6]

The strength of the coupling between the soft Fe layer and the hard FePt layer and the validity of our model were further investigated by means of magnetization measurements. That is, time spectra are recorded in external fields in the range of 0–5.6 T while the synchrotron beam was fixed at certain positions on the probe layer. Two positions on the wedge are selected, corresponding to a distance of 1.4 and 5.4 nm to the FePt interface. The field was directed parallel to the in-plane bcc-Fe[110] direction and thus, at saturation the moments are expected to align with this direction. As a consequence, the magnetic moments have an additional degree of rotation in the thin-film plane.

A selection of time spectra recorded on the bilayer in an external field are shown in Figs. 5(a) and 5(b). For both positions of the probe layer, the spectra recorded in a field of 3.5 T look similar. However, in a field of 1.0 T the moments in the probe layers behave differently. At a probe distance of 1.4 nm to the interface the spectrum is comparable to the low-field spectrum whereas at a distance of 5.4 nm the spectrum shows more similarities with the spectrum obtained in a field of 3.5 T. A more detailed analysis of all spectra allows us to reconstruct the magnetic moment orientation as a function of the external field. The angles ϕ and θ are plotted as a function of the external field in Figs. 5(c) and 5(d), respectively. A three-dimensional representation of the moment ro-

tation is given in Figs. 5(e) and 5(f). For $\theta < 20°$ it is difficult to obtain a unique value of ϕ as in this region, $m(\theta, \phi = 0°)$ is almost identical to $m(\theta, \phi = 45°)$. This is the case for the low-field measurements obtained with the beam pointed in the beginning of the wedged probe layer ($d = 1.4$ nm). Therefore no value for ϕ is given in this field region. When no error bar is indicated in Fig. 5(c), the angle was kept fixed during the fitting process.

A small field on the order of ~ 100 mT is needed to rotate the moments toward $\phi = 0°$ which corresponds with a magnetic harder direction. This effect can be attributed to the magnetocrystalline anisotropy of bcc-Fe.

The moments of the probe layers located at 1.4 and 5.4 nm from the FePt interface gradually rotate from canted out of the film plane toward the plane of the thin film. At a field of 5.6 T the moments at a distance of 1.4 nm from the interface are nearly saturated in the thin-film plane whereas for $d = 5.4$ nm saturation ($\theta \approx 90°$) is reached at 4.5 T.

To demonstrate the significance of the exchange coupling constant J as the relevant parameter for the exchange-spring behavior, simulation results obtained with exchange-spring constants in the range of $0.2 \times 10^{-11} - 3.0 \times 10^{-11}$ J/m are shown in panels (c) and (d) of Fig. 5. $J = 2.0 \times 10^{-11}$ J/m gives the best match with both magnetization curves. The micromagnetic simulations show that the strength of the exchange coupling constant J strongly influences the spring stiffness as well as the critical thickness at which the transition from rigid magnet to exchange spring occurs. The remaining deviations of the simulated curves from the experimental data may be attributed to the adopted approximations of the model. For example, in our model we do not discriminate between the exchange coupling between two adjacent Fe sublayers and the coupling between Fe and FePt at the interface ($J_{\text{Fe-Fe}} = J_{\text{Fe-FePt}}$). Second, the FePt thin film is considered as one single rigid magnet, not allowing for spin canting within the FePt film. Third, possible effects of strain relaxation and related variations in the magnetostriction in the Fe film due to the epitaxial mismatch[32] to the FePt underlayer are not considered. Nevertheless, the major features of the experimental observations, both the thickness dependence as well as the field dependence, are qualitatively well reproduced with the simple micromagnetic model. This demonstrates that the exchange interaction within the Fe layer is the key mechanism that determines the spin orientation in the soft magnetic layer of the bilayer system.

Both the zero- and the nonzero-field measurements indicate that the spins behave like an exchange spring in the orthogonal direction for Fe-FePt bilayers with a total soft-layer thickness ≥ 4.1 nm, which is the sum of the three sublayers of the wedge: ^{56}Fe(2.8 nm)/^{57}Fe(0.7 nm)/^{56}Fe(0.6 nm). At zero field the Fe moments in the top monolayers are canted away from the sample normal. Consequently, the remanent magnetization of the total bilayer in the perpendicular direction is lower than the saturation magnetization. This experimental result is in agreement with the macroscopic magnetization curves of Fe(x)-FePt bilayers reported by Casoli *et al.*[5] There, depending on the thickness of the soft phase two coupling regimes were observed, i.e., the rigid magnet regime and the exchange-spring regime.[6] The rigid magnet is characterized by a square loop with high remanence and by a single critical magnetization reversal field whereas the exchange-spring bilayer shows a magnetization loop with reduced remanence and the inversion of its magnetization starts in the first quadrant. In that work, a critical thickness for the Fe layer of ~ 2 nm is experimentally identified for the transition from the rigid magnet to the exchange-spring magnet regime. We found that for a soft layer with a thickness less than 3.3 nm the Fe moments are aligned with the easy axis of the $L1_0$-FePt layer and the bilayer behaves like a rigid magnet.

IV. CONCLUSIONS

We have studied the magnetization direction in the top layer of the soft Fe layer in an Fe-FePt bilayer as a function of the Fe-layer thickness. The bcc-Fe layer, which tends to align its magnetization in the thin-film plane, is exchanged coupled to an $L1_0$-FePt layer of which the magnetization is perpendicular to the film plane. We identified an exchange-spring behavior on the microscopic scale by locally probing an ultrathin ^{57}Fe layer with nuclear-resonant scattering of synchrotron radiation. The Fe-moment rotation is quantified in the perpendicular direction. That is, the Fe moments gradually cant away from the sample normal as the thickness of the Fe layer increases. In addition, we performed magnetometry measurements to investigate the strength of the exchange coupling with the external field applied along the in-plane Fe[110] direction. From the NRS time spectra we could deduce that the field required to cant the moments toward the external field decreases as the distance from the interface increases. Finally, our one-dimensional micromagnetic simulations show that the spring stiffness and the critical thickness at which the transition from rigid magnet to exchange spring occurs is determined by the strength of the exchange coupling constant J within the Fe layer of the Fe-FePt bilayer system with $J = 2.0 \times 10^{-11}$ J/m.

ACKNOWLEDGMENTS

We wish to thank the staff at the ESRF beamline ID18 cordially for their help during the experiment. The work was supported by FWO (Fund for Scientific Research Flanders), by the Concerted Action of the K.U. Leuven (Grant No. GOA/09/006), by the K.U.Leuven CREA/07/006 program, by the Interuniversity Attraction Pole (Grant No. IAP P6/42) and by the Centers of Excellence Programme (Grant No. INPAC EF/05/005).

*bart.laenens@imec.be

[1] E. F. Kneller and R. Hawig, IEEE Trans. Magn. **27**, 3588 (1991).
[2] R. Skomski and J. M. D. Coey, Phys. Rev. B **48**, 15812 (1993).
[3] H. Zeng, J. Li, J. P. Liu, Z. L. Wang, and S. Sun, Nature (London) **420**, 395 (2002).
[4] R. Röhlsberger, H. Thomas, K. Schlage, E. Burkel, O. Leupold, and R. Rüffer, Phys. Rev. Lett. **89**, 237201 (2002).
[5] F. Casoli, F. Albertini, S. Fabbrici, C. Bocchi, L. Nasi, R. Ciprian, and L. Pareti, IEEE Trans. Magn. **41**, 3877 (2005).
[6] G. Asti, M. Ghidini, R. Pellicelli, C. Pernechele, M. Solzi, F. Albertini, F. Casoli, S. Fabbrici, and L. Pareti, Phys. Rev. B **73**, 094406 (2006).
[7] G. H. O. Daalderop, P. J. Kelly, and M. F. H. Schuurmans, Phys. Rev. B **44**, 12054 (1991).
[8] T. Klemmer, D. Hoydick, H. Okumura, B. Zhang, and W. A. Soffa, Scr. Metall. Mater. **33**, 1793 (1995).
[9] E. E. Fullerton, J. S. Jiang, M. Grimsditch, C. H. Sowers, and S. D. Bader, Phys. Rev. B **58**, 12193 (1998).
[10] J. S. Jiang and S. D. Bader, Mater. Sci. Technol. **17**, 1491 (2001).
[11] K. V. O'Donovan, J. A. Borchers, C. F. Majkrzak, O. Hellwig, and E. E. Fullerton, Phys. Rev. Lett. **88**, 067201 (2002).
[12] V. E. Kuncser, M. Doi, W. Keune, M. Askin, H. Spies, J. S. Jiang, A. Inomata, and S. D. Bader, Phys. Rev. B **68**, 064416 (2003).
[13] T. Shima, K. Takanashi, Y. K. Takahashi, and K. Hono, Appl. Phys. Lett. **81**, 1050 (2002).
[14] K. Barmak, J. Kim, L. H. Lewis, K. R. Coffey, M. F. Toney, A. J. Kellock, and J. U. Thiele, J. Appl. Phys. **98**, 033904 (2005).
[15] B. Laenens, C. Rentenberger, M. Rennhofer, F. Almeida, N. Planckaert, B. Sepiol, K. Temst, J. Meersschaut, and A. Vantomme, J. Appl. Phys. **105**, 073913 (2009).
[16] A. Cebollada, D. Weller, J. Sticht, G. R. Harp, R. F. C. Farrow, R. F. Marks, R. Savoy, and J. C. Scott, Phys. Rev. B **50**, 3419 (1994).
[17] R. F. C. Farrow, D. Weller, R. F. Marks, M. F. Toney, A. Cebollada, and G. R. Harp, J. Appl. Phys. **79**, 5967 (1996).
[18] J. U. Thiele, S. Maat, J. L. Robertson, and E. E. Fullerton, Appl. Phys. Lett. **82**, 2859 (2003).
[19] J. U. Thiele, S. Maat, and E. E. Fullerton, IEEE Trans. Magn. **40**, 2537 (2004).
[20] S. M. Watson, T. Hauet, J. A. Borchers, S. Mangin, and E. E. Fullerton, Appl. Phys. Lett. **92**, 202507 (2008).
[21] F. Casoli, F. Albertini, L. Nasi, S. Fabbrici, R. Cabassi, F. Bolzoni, and C. Bocchi, Appl. Phys. Lett. **92**, 142506 (2008).
[22] G. Asti, M. Solzi, M. Ghidini, and F. M. Neri, Phys. Rev. B **69**, 174401 (2004).
[23] D. Suess, T. Schrefl, R. Dittrich, M. Kirschner, F. Dorfbauer, G. Hrkac, and J. Fidler, J. Magn. Magn. Mater. **290-291**, 551 (2005).
[24] C. L'abbé, J. Meersschaut, W. Sturhahn, J. S. Jiang, T. S. Toellner, E. E. Alp, and S. D. Bader, Phys. Rev. Lett. **93**, 037201 (2004).
[25] N. Planckaert, C. L'abbé, B. Croonenborghs, R. Callens, B. Laenens, A. Vantomme, and J. Meersschaut, Phys. Rev. B **78**, 144424 (2008).
[26] T. Diederich, S. Couet, and R. Röhlsberger, Phys. Rev. B **76**, 054401 (2007).
[27] R. Rüffer and A. I. Chumakov, Hyperfine Interact. **97-8**, 589 (1996).
[28] S. S. Hanna, J. Heberle, G. J. Perlow, R. S. Preston, and D. H. Vincent, Phys. Rev. Lett. **4**, 513 (1960).
[29] W. Sturhahn, Hyperfine Interact. **125**, 149 (2000).
[30] N. Papanicolaou, J. Phys.: Condens. Matter **10**, L131 (1998).
[31] J. Meersschaut, C. L'abbé, F. M. Almeida, J. S. Jiang, J. Pearson, U. Welp, M. Gierlings, H. Maletta, and S. D. Bader, Phys. Rev. B **73**, 144428 (2006).
[32] B. Croonenborghs, F. M. Almeida, S. Cottenier, M. Rots, A. Vantomme, and J. Meersschaut, Appl. Phys. Lett. **85**, 200 (2004).